Developmental Biology **209,** 221–238 (1999)
Article ID dbio.1999.9249, available online at http://www.idealibrary.com on IDEAL®

Measurements of Mechanical Properties of the Blastula Wall Reveal Which Hypothesized Mechanisms of Primary Invagination Are Physically Plausible in the Sea Urchin *Strongylocentrotus purpuratus*

L. A. Davidson,*,[1] G. F. Oster,† R. E. Keller,‡ and M. A. R. Koehl§

**Graduate Group in Biophysics, University of California at Berkeley, Berkeley, California 94720; †Department of Molecular and Cell Biology, University of California at Berkeley, Berkeley, California 94720; ‡Department of Biology, University of Virginia, Charlottesville, Virginia 22903; and §Department of Integrative Biology, University of California at Berkeley, Berkeley, California 94720*

Computer simulations showed that the elastic modulus of the cell layer relative to the elastic modulus of the extracellular layers predicted the effectiveness of different force-generating mechanisms for sea urchin primary invagination [L. A. Davidson, M. A. R. Koehl, R. Keller, and G. F. Oster (1995) *Development* 121, 2005–2018]. Here, we measured the composite elastic modulus of the cellular and extracellular matrix layers in the blastula wall of *Strongylocentrotus purpuratus* embryos at the mesenchyme blastula stage. Combined, these two layers exhibit a viscoelastic response with an initial stiffness ranging from 600 to 2300 Pa. To identify the cellular structures responsible for this stiffness we disrupted these structures and correlated the resulting lesions to changes in the elastic modulus. We treated embryos with cytochalasin D to disrupt the actin-based cytoskeleton, nocodazole to disrupt the microtubule-based cytoskeleton, and a gentle glycine extraction to disrupt the apical extracellular matrix (ECM). Embryos treated less than 60 min in cytochalasin D showed no change in their time-dependent elastic modulus even though F-actin was severely disrupted. Similarly, nocodazole had no effect on the elastic modulus even as the microtubules were severely disrupted. However, glycine extraction resulted in a 40 to 50% decrease in the elastic modulus along with a dramatic reduction in the hyalin protein at the apical ECM, thus implicating the apical ECM as a major mechanical component of the blastula wall. This finding bears on the mechanical plausibility of several models for primary invagination.

Key Words: **mechanics; primary invagination; sea urchin; gastrulation.**

INTRODUCTION

Forces exerted by cells and tissues interact with the mechanical properties of embryonic tissue to drive morphogenesis. Yet, few studies have attempted physical measurements of mechanical properties relevant to morphogenesis. Epithelial bending is a common morphogenetic process during animal development (Ettensohn, 1985b). In the sea urchin, an early case of epithelial bending accompanies primary invagination as the flat vegetal plate bends inward to form the primitive gut. Primary invagination is driven by physical forces acting within the vegetal plate of the late mesenchyme blastula stage embryo (Ettensohn, 1984a; Kimberly and Hardin, 1998; Moore and Burt, 1939). The spatial and temporal pattern of those forces and the physical properties of the embryo determine the course of invagination and the resultant shape of the archenteron. Yet, despite a century of work on the many participating genes, the kinematics of tissue movements, the ultrastructure of the cytoskeleton and extracellular matrix, and the patterning of cell fates involved in invagination, there is still no answer to the question: How do sea urchins invaginate? The optical

[1] To whom correspondence should be addressed at Department of Biology, Gilmer Hall, University of Virginia, Charlottesville, VA 22903. Fax: (804) 982-5626. E-mail: lad4x@virginia.edu.

0012-1606/99 $30.00

clarity of the sea urchin embryo at these stages as well as the accessibility to its mechanical structures makes the sea urchin embryo an excellent system to study the basic mechanics of epithelial bending.

During primary invagination, the archenteron is formed as the flat vegetal plate bends inward to form a shallow pit. As the archenteron deepens between 5 and 10 μm, the smooth apical surface of the archenteron changes shape from a pit to a tube with a flat roof (Amemiya, 1989; Ettensohn, 1984b; Kimberly and Hardin, 1998). Primary invagination ends as secondary mesenchyme cells at the tip of the archenteron send protrusions into the blastocoel (Miller *et al.*, 1995) and the archenteron continues to extend across the blastocoel toward the animal pole (Ettensohn, 1985a; Hardin and Cheng, 1986).

Primary invagination frequently fails when the extracellular matrix (ECM) is perturbed but is relatively robust to disruption of the cytoskeleton (see Lane *et al.*, 1993, for an overview). Blocks to matrix biosynthesis, inhibitors of secretion, or antibodies against apical ECM components can block or cause abnormal invagination (Alliegro *et al.*, 1992; Burke and Tamboline, 1990; Butler *et al.*, 1987; Lane *et al.*, 1993; Wessel and McClay, 1987). In contrast, inhibitors of microtubules have no effect (Hardin, 1987) and cytochalasin D, an inhibitor of F-actin, has no apparent effect when applied immediately before invagination (Lane *et al.*, 1993); Nakajima and Burke (1996) report that early application of cytochalasin does block gastrulation. The role of the ECM is complex and defects in synthesis could affect cell signaling pathways (Ramachandran *et al.*, 1993, 1997) as well as the mechanical function of the ECM required for gastrulation.

We apply mechanical engineering principles to understand how cells and tissues interact physically during invagination and the mechanical consequences of this interaction. Most textbooks on cell and developmental biology attribute mechanical properties to these components, acknowledge their contributions to the structural integrity of tissues, and often infer roles in morphogenesis. The ultrastructure and biochemical constitution of the sea urchin embryo, the filamentous nature of its cytoskeleton, the junctional complexes between its cells, and its extracellular matrices have been extensively characterized (Hawkins *et al.*, 1995; Miller and McClay, 1997a,b; Nakajima and Burke, 1996; Wessel *et al.*, 1998). An early effort was made to evaluate the force required to arrest invagination in the starfish using osmotic pressure (Moore, 1941). Additionally, Gustafson and Wolpert (1963) reported using the Mitchison and Swann "cell elastimeter" (Mitchison and Swann, 1954) to measure the stiffness of the blastula wall in the sea urchin *Psammechinus miliaris.* Since these early studies numerous advances in the cell biology of the cytoskeleton and the extracellular matrix have developed reagents that now allow us to investigate their roles in the mechanics of primary invagination. Ours is the first comprehensive effort to measure mechanical properties of the embryo that are relevant to the mechanical processes driving primary invagination in the sea urchin embryo.

A number of physical mechanisms have been hypothesized to drive primary invagination [for review, see Davidson *et al.* (1995), Kimberly and Hardin (1998), and Nakajima and Burke (1996)]. Our computer simulations showed that the ability of a mechanism to create a pit depended on the elastic modulus (i.e., stiffness) of the cell layer relative to the stiffness of the apical ECM within the blastula wall (Davidson *et al.*, 1995). A material's stiffness is its resistance to deformation when subjected to stress. Stress is defined as the force per cross-sectional area of the material bearing that force. Strain is a dimensionless measure of deformation, such as a change in length divided by the un-deformed length (for details, see Wainwright *et al.*, 1976). Forces acting on tissues with low stiffness will produce larger strains than the same forces acting on tissues with high stiffness. Our computer simulations demonstrated that models of the cell tractoring toward the center of the vegetal plate, apicobasal contraction, and ECM gel swelling of cells within the vegetal plate simulate primary invagination only when the apical ECM is very stiff relative to the cell layer. Alternatively, models of the apical constriction of cells within the vegetal plate or an apical contractile ring through cells surrounding the vegetal plate work only when the stiffness of the apical ECM layer is of similar or lower stiffness than the cell layer.

Here we use the compression techniques developed by Hiramoto (1990) to measure the stiffness of the blastula wall, a structure that combines the cellular epithelium and apical ECM, in the sea urchin embryo at the mesenchyme blastula stage. To address the question of whether the stiffness arises from the cell layer or from the apical ECM, we measure the stiffness of embryos treated with cytochalasin D to depolymerize the actin-based cytoskeletal network of the cell layer, embryos treated with nocodazole to depolymerize the microtubule-based cytoskeleton of the cell layer, and embryos extracted with glycine to remove the hyaline layer from the apical ECM. We show that the stiffness of the blastula wall is derived from apical ECM which is at least five times stiffer than the cell layer. These findings suggest that (i) neither the apical constriction nor the apical contractile ring hypothesis is capable of driving primary invagination in the sea urchin *Strongylocentrotus purpuratus;* and (ii) the remaining hypotheses, cell tractoring, apicobasal contraction, and apical ECM swelling, are all physically capable of driving primary invagination.

MATERIALS AND METHODS

Culture of Embryos

Adult *S. purpuratus* (collected near Point Arena, CA, or supplied by Marinus, Long Beach, CA) were induced to spawn and embryos were cultured and staged as described by Lane *et al.* (1993). All experiments were carried out on embryos from 2 to 6 h after hatching from their fertilization membrane.

Histology

Embryos were fixed differently to visualize the actin-based cytoskeleton, the microtubule-based cytoskeleton, and the hyalin protein-based apical extracellular matrix. To visualize F-actin, live embryos were fixed for 10 min on ice with acetone and 0.8 mM TRITC-labeled phalloidin (P-5157, Sigma). To visualize microtubules, embryos were fixed for 1 h on ice with Gard's fixative (Gard, 1991). Fixed embryos were stored at −20°C in 100% methanol. Autofluorescence was reduced by a 12- to 24-h incubation with 100 mM $NaBH_4$ in PBS. After the reduction step, embryos were processed for indirect immunofluorescence (Miller and McClay, 1997b) using antibodies to β-tubulin (1:1000; Boehringer-Mannheim). To visualize the apical extracellular matrix, we fixed embryos for 15 min on ice with Dent's fixative (Dent *et al.,* 1989). These embryos were then processed for indirect immunofluorescence using antibodies to hyalin protein (1:10; UH2-183, D. McClay). Images of labeled embryos were collected with a confocal laser-scanning microscope (FXV-1000, Olympus).

Preparation of Needles for Stiffness Measurement

Needles of varying stiffness were pulled with a needle puller (David Kopf Instruments or Sutter Instruments). Needles were selected with a flexural stiffness high enough to deform the embryo but low enough that the amount they bent could be measured accurately. Small square pieces of mica (Ted Pella Microscope Supplies), hand cut to approximately 300 × 300 × 20 μm, were glued to the tips of the needles with a cyanoacrylate adhesive. A small number of needles with mica tips were calibrated by hanging known weights (small pieces of thin wire) from their tips and measuring the displacement. These calibrated needles were then used to calibrate the mica-tipped needles used in the compression experiments. Needles used for compression tests required 10 to 30 nNewtons to produce a 1-μm lateral displacement of the needle tip.

Measurement of Mechanical Properties

Compression tests were conducted in a chamber constructed from an acrylic ring (24 by 50 mm) sandwiched between two pieces of glass coverslip with silicone grease (Dow Corning). A backstop, to prevent embryos from moving when compressed by the needle, was made by gluing a coverslip fragment to the surface of the bottom coverslip. The top coverslip was set off to one side to allow the mica-tipped needle into the chamber and still allow the use of DIC optics. The chamber was filled with approximately 2 ml of seawater and placed on the microscope stage of an inverted microscope (Nikon) at room temperature (20°C). The microneedle was then positioned less than 100 μm from the backstop. Embryos concentrated in SW were then added to the chamber to bring the concentration to approximately 1000 embryos per milliliter. Embryos were then selected at random for compression and gently trapped between the mica and the backing. Once an embryo was trapped, the base of the microneedle was moved 30 μm in approximately 0.5 s with a micromanipulator (Narashige), compressing the embryo. The time course of the compression was recorded to video tape (Hammatsu XC-77 CCD camera) for 2 min before the embryo was released.

Compression tests were carried out at the same temperature since viscoelastic properties can depend on temperature (Wainwright *et al.,* 1976). Since embryos were cultured at 15°C and compression tests carried out at 20°C, we assumed that the cell layer and ECM layers changed properties equally. Once a set of compression tests were complete, embryos were returned to 15°C and in all cases control embryos gastrulated normally.

For most experiments the *S. purpuratus* embryos were deciliated an hour prior to the compression test so that they could be captured. Deciliation was carried out as described by Burke *et al.* (1991) and had no effect on measured stiffness (40 control and 43 deciliated embryos from five cultures; $P = 0.074$ by two-way ANOVA; see Statistical Analyses below).

Determination of Time-Dependent Stiffness

Many biological materials are viscoelastic; hence, the stiffness decreases with time as they bear a load (Wainwright *et al.,* 1976). The creep test and the stress-relaxation test are two standard protocols for the determination of the time-dependent stiffness of a material (e.g., Findley *et al.,* 1989). The creep test begins with the imposition of a constant stress on a sample of the material, and strain increases with time. The stress-relaxation test begins with the imposition of a constant strain on the sample, and stress decreases with time. The compression tests carried out below are a hybrid of the creep test and the stress-relaxation test. At the start of compression, the base of the microneedle was moved 30 μm and remained there for the rest of the test. The applied force depended on the displacement of the microneedle tip from the base as the whole needle bent. As the embryo deformed (i.e., strain changed), the position of the tip of the microneedle also changed (i.e., stress changed). Thus, measurements of the time-dependent stiffness were carried out as both the stress and strain changed in the embryo.

Microneedle position and the deformation of compressed embryos were measured from the video recordings of each compression test (Peak Performance Technologies Inc. or the public domain NIH-Image program). Single frames were sampled from the video immediately before compression and every 10 s thereafter. Figures 1A and 1B show a control embryo before and during compression. The positions of 14 landmark points (marked by x's in Fig. 1B) were digitized for each frame. The location of these landmarks ($\pm$3 μm) allowed the determination of R_0, R_1, R_2, and R_C (defined in Fig. 1C). The force of compression, F, was determined by the lateral deflection of the mica tip of the microneedle relative to the position of the needle base. These values combined with an approximate thickness for the blastula wall of 10 μm (as measured from live embryos subjected to the compression test) and an assumed initial strain of 10% (blastula stage embryos pierced with a needle deflate slightly as if pressurized; thus, an initial strain of 10% was chosen to reflect this pre-pressurization) were used with the equations developed by Hiramoto (1963) to calculate the stiffness for the blastula wall at 10-s intervals. The mean stiffness after 10 s of compression (E_{10}) of several embryos from each culture or each treatment was calculated as summarized in the Appendix.

The sea urchin blastula, like most biological materials (Wainwright *et al.,* 1976), does not behave as a simple elastic solid but instead exhibits both fluid- and elastic-like behaviors in response to compression. How such a "viscoelastic" material changes shape and resists compression depends on the rate, amount, and history of the compressive load and can be modeled mathematically as a collection of springs and dashpots (Findley *et al.,* 1989). By measuring the elastic response over a short-term compression, a set of parameters can be calculated that assign values to such a collection of springs and dashpots so that the springs and dashpots empirically match the behavior of the material over the short-term compression and predict the behavior over longer periods of compression.

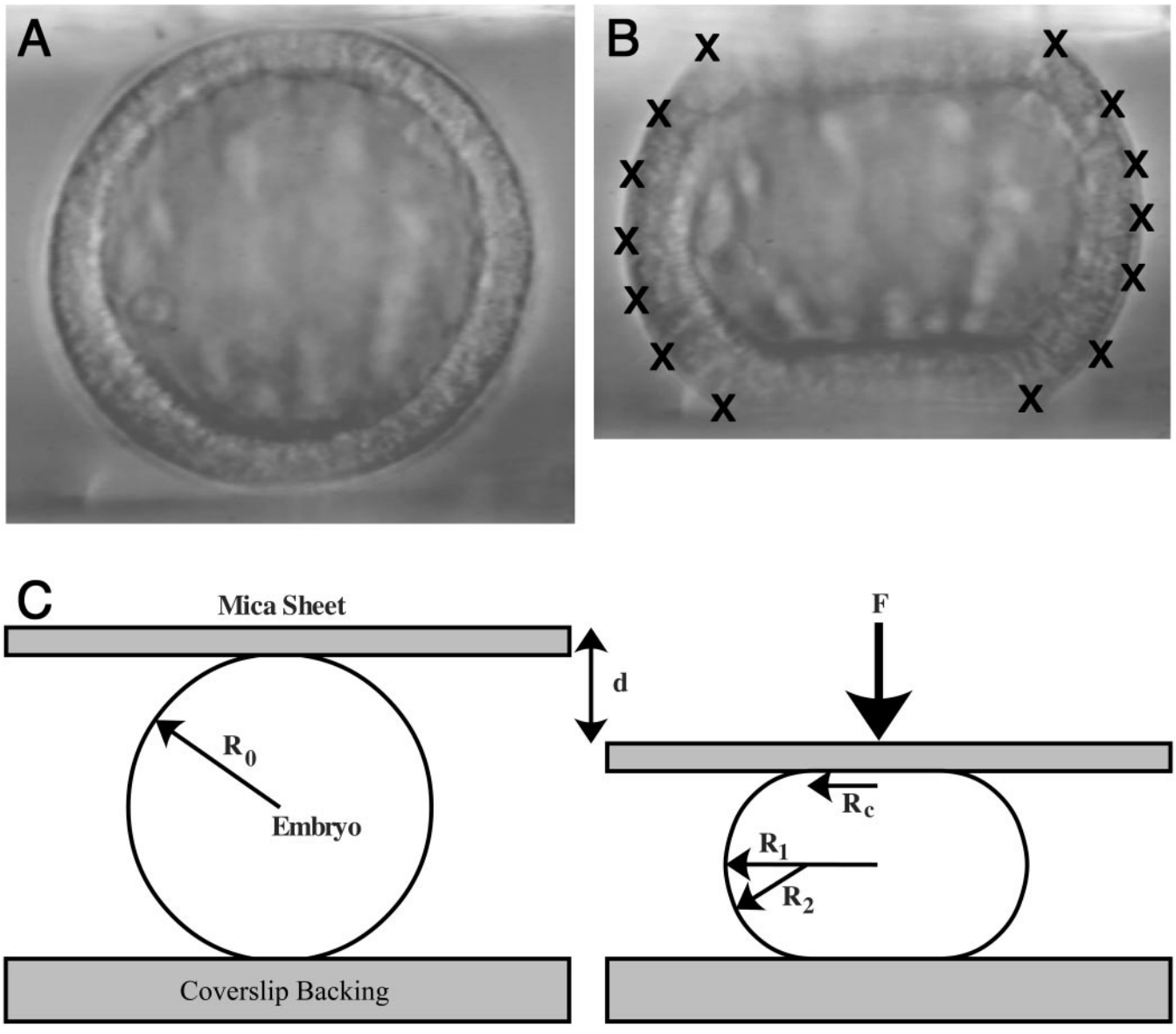

FIG. 1. A compression test of a *S. purpuratus* embryo at the mesenchyme blastula stage. (A) Before compression, an embryo is gently trapped between a mica sheet (attached to the microneedle) and a coverslip backing. As force is applied to the embryo through contact areas with the backing and the mica sheet, pressure within the blastocoel increases, and the blastula wall which is under tension expands. During compression, the shape of the embryo reflects the mechanical balance between the pressure within the blastocoel and the tension in the blastula wall. Thus, compression of the whole embryo under the microneedle generates additional tension in the blastula wall, a composite of a sheet of cells and layers of ECM. (B) Recognizable landmarks, which are indicated with x's on the compressed embryo, are digitized: contact points with the mica and coverslip, the equator of the compressed embryo, and locations along the meridian of the embryo. (C) The initial radius, R_0, is measured before compression begins. The features measured or calculated for any time point in the course of compression were d, mica sheet displacement; F, the force of compression; R_c, the radius of the contact area; R_1, the circumferential radius of the embryo; and R_2, the meridian radius of the embryo.

Thus, we can compare the results of different experiments using either the elastic response at specific times after compression or the parameters calculated from that response.

To compare the stiffness of the blastula wall subjected to different treatments we chose the stiffness 10 s after the onset of compression (E_{10}) for several reasons. First, the use of calibrated microneedles limits the experimental resolution of the smaller compression forces at significantly longer times. Second, the short

duration assured that we were measuring the mechanical response of the cell and apical ECM layers to a load unconfounded by the leakage of fluid out of the blastocoel that might have occurred after longer times, i.e., that the stiffness we measured reflected the stiffness of the cell and apical ECM layers rather than their hydraulic conductivity. We did not choose shorter durations because we wanted to minimize the effects of slight variations in loading rate at the onset of each trial. We chose the posthatching blastula because their spherical shape was more conducive for mathematical analysis. Stiffness of the blastula wall did not change between 2 and 6 h after hatching (data not shown). Tests for significant difference between controls and treated sets within the same culture were done using the Mann–Whitney *U* test (Sokal and Rohlf, 1981) while tests for significant differences between controls and treated sets across all cultures were carried out using the two-way ANOVA test (SAS version 6.09, SAS Institute Inc.).

Curve Fitting to Spring-and-Dashpot Mechanical Equivalents

The empirically determined viscoelastic response of the embryo's tissue can be represented by a mechanically equivalent set of ideal springs to model the tissue's elastic behavior and dashpots to model the tissue's viscous behavior (e.g., Koehl, 1990). The standard linear model (Findley *et al.,* 1989) for viscoelastic response combines a single spring element in parallel with a spring and dashpot element in series (see Fig. 2A). Values for the spring constants and the coefficient of viscosity were determined as described in Moore *et al.* (1995).

Determination of Embryo Volume and Initial Strain of the Blastula Wall

The mathematical model we used to calculate the stiffness of the blastula wall assumes that the volume of fluid in the blastocoel remains constant while an embryo is compressed. We tested that assumption by measuring the volume of compressed embryos over the course of each experiment. Video and time-lapse recordings were collected during the experiments as above. Positions of 14 landmarks (x's marked in Fig. 1B) on the compressed embryos were digitized. These landmarks on the embryo's surface allowed the construction of a spline function fitting the form of the embryo's wall. The volume was then calculated for the solid of revolution enclosed as the spline function was rotated about the embryo's axis of compression (Fig. 1D).

The mathematical model we used to calculate the stiffness of the blastula wall assumes that embryos at the blastula stage are slightly "inflated" (i.e., prestrained) and that the amount of inflation does not differ from treatment to treatment (see Appendix). We tested that assumption by measuring the change in embryo circumference after *S. purpuratus* embryos were punctured with a fine glass needle. Video and time-lapse recordings were collected as above and the circumference of the blastula wall of these embryos was measured as they were pierced.

Treatment of Embryos with Cytochalasin D and Nocodazole

Cytochalasin D was chosen for its clear effects on the actin cytoskeleton (Schliwa, 1982), the speed and selectivity of its effects (Rao *et al.,* 1992), and its ability to reduce the cortical stiffness in isolated cells (Ting-Beall *et al.,* 1995). Nocodazole was chosen for its speed of action and specificity against microtubules, which have been identified as playing a central role in cell stiffness (Gittes *et al.,* 1993; Wang *et al.,* 1993). Treatments consisted of culturing 6 ml of dilute cultures (1500 embryos per milliliter SW) in 6 μM cytochalasin D (Sigma) or 40 μM nocodazole (Sigma). Control embryos were treated with either ethanol or DMSO (tissue culture grade DMSO, Sigma) alone to the same dilution as used on treated embryos. Embryos prepared for histology were fixed 30 min after treatment with cytochalasin D or 60 min after treatment with nocodazole.

Glycine Extraction of Embryos

Glycine extraction was chosen to remove the apical extracellular matrix. Glycine extraction has more typically been used to biochemically isolate hyalin protein and other constituent proteins and glycoproteins of the apical ECM (Alliegro and McClay, 1988; Kane, 1973; McClay and Fink, 1982); here a modification of the protocol used for biochemical isolation of hyaline layer proteins (McClay and Fink, 1982) allowed the embryos to recover and develop normally. Embryos were washed once in calcium- and magnesium-free seawater (CMFSW) and were then placed for 2 min in a solution of one part hyalin extraction media (HEM) to two parts CMFSW. HEM stocks consisted of 0.3 M glycine, 0.3 M NaCl, 10 mM KCl, 10 mM $MgSO_4$, 10 mM Tris, 2 mM EGTA and were and balanced with NaOH to pH 8. This gentle extraction leaves most embryos intact. Extracted embryos were then washed extensively in seawater and allowed to recover for an hour before either the compression experiments or fixation for histology.

RESULTS

During the compression test, the shape of the embryo reflects the mechanical balance between the pressure within the blastocoel and the tension in the blastula wall. Using microneedles, we have measured the time-dependent stiffness of the blastula wall of control embryos from 19 different cultures (culture refers to a set of sibling embryos fertilized from the gametes of the single male and single female). Figure 2B illustrates the results of 12 control embryos from a single culture. While there can be a twofold variation in the E_{10} within a single culture, a fourfold variation in the E_{10} can be seen from culture to culture (see Fig. 3A). The source of this culture-to-culture variability is likely to reflect the natural variation in the population of adult sea urchins; other sources of variation have been ruled out, including: the possibility of strain hardening (see Fig. 3B), systematic errors due to digitization and analysis, differences in needles used for compression, embryo orientation (i.e., variation in the stiffness between the vegetal plate and the blastocoel wall), and embryonic stage (data not shown). These stiffnesses reflect the combined stiffness that the cell layer and the apical extracellular matrix contribute to the blastula wall. To establish relative contributions of these layers we next attempted to undermine the mechanical contributions of the individual layers.

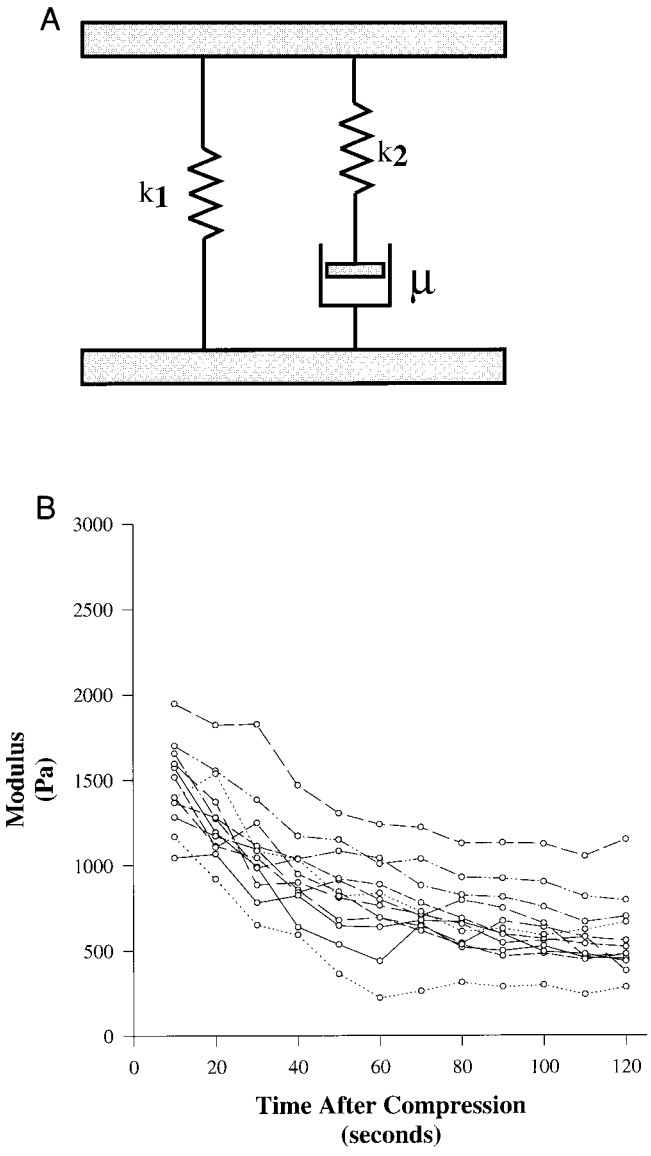

FIG. 2. Time dependence of composite stiffness. (A) The standard linear model of viscoelastic response. An ideal spring element (spring constant k_1) is in parallel with a series ideal spring (spring constant k_2) and an ideal dashpot (coefficient of viscosity μ). When a force is applied to a spring, it instantaneously deforms, and when the force is removed, it instantaneously snaps back to its original length; the amount of deformation is proportional to the force applied. In contrast, when a force is applied to a dashpot, it deforms at a rate that is proportional to the magnitude of the force applied, and when the force is removed, the dashpot remains extended. (B) $E(t)$ vs t for a set of 12 control *S. purpuratus* embryos from culture #1 (see Table 1). The time-dependent stiffness can be modeled by the spring and dashpot configuration in A. At the start of compression the stiffness of the composite is simply the sum of the two springs $[k_1 + k_2]$. Over the course of the compression test, the dashpot deforms to release forces acting on the second spring, k_2, until only the first spring, k_1, remains deformed. Thus, $[k_1 + k_2]$ reflects the initial stiffness, while k_1 reflects the value of the long-term stiffness. The coefficient of viscosity, μ, determines how quickly the stiffness changes from $[k_1 + k_2]$ to k_1.

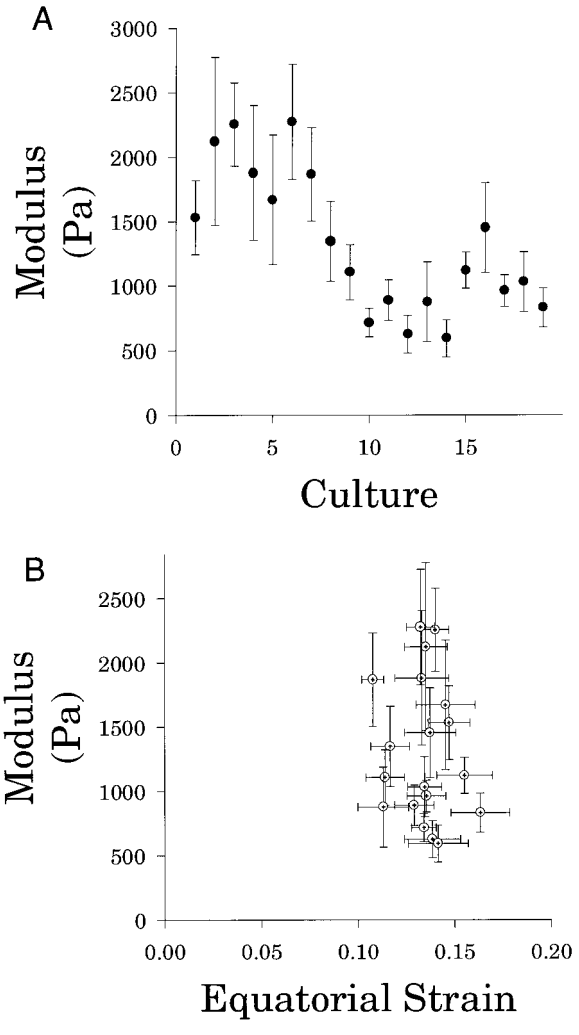

FIG. 3. Between-culture variation of stiffness in *S. purpuratus* embryos from blastula and mesenchyme blastula stages. (A) Variability from culture to culture of the mean stiffness after 10 s of compression (E_{10}). (B) Mean stiffness (E_{10}) versus mean circumferential strain after 10 s of compression. If the blastula wall exhibited strain hardening, i.e., an increase in measured stiffness with an increase in applied strain, these points would fall on a line with a positive slope. (Error bars indicate ±1 SD.)

FIG. 4. Effects of cytochalasin D, nocodazole, and glycine extraction on the distribution of F-actin, microtubules, and the hyalin layer in mesenchyme blastula stage embryos. Confocal sections through (A, B, and C) control embryos, (D, E, and F) embryos treated with cytochalasin D for 30 min, (G, H, and I) embryos treated with nocodazole for 60 min, and (J, K, and L) glycine-extracted embryos after 60 min of recovery in seawater. Note in E that cytochalasin D also disrupts microtubules. M shows an embryo prepared for F-actin but not incubated with TRITC phalloidin. N and O show embryos fixed and prepared without primary antibody.

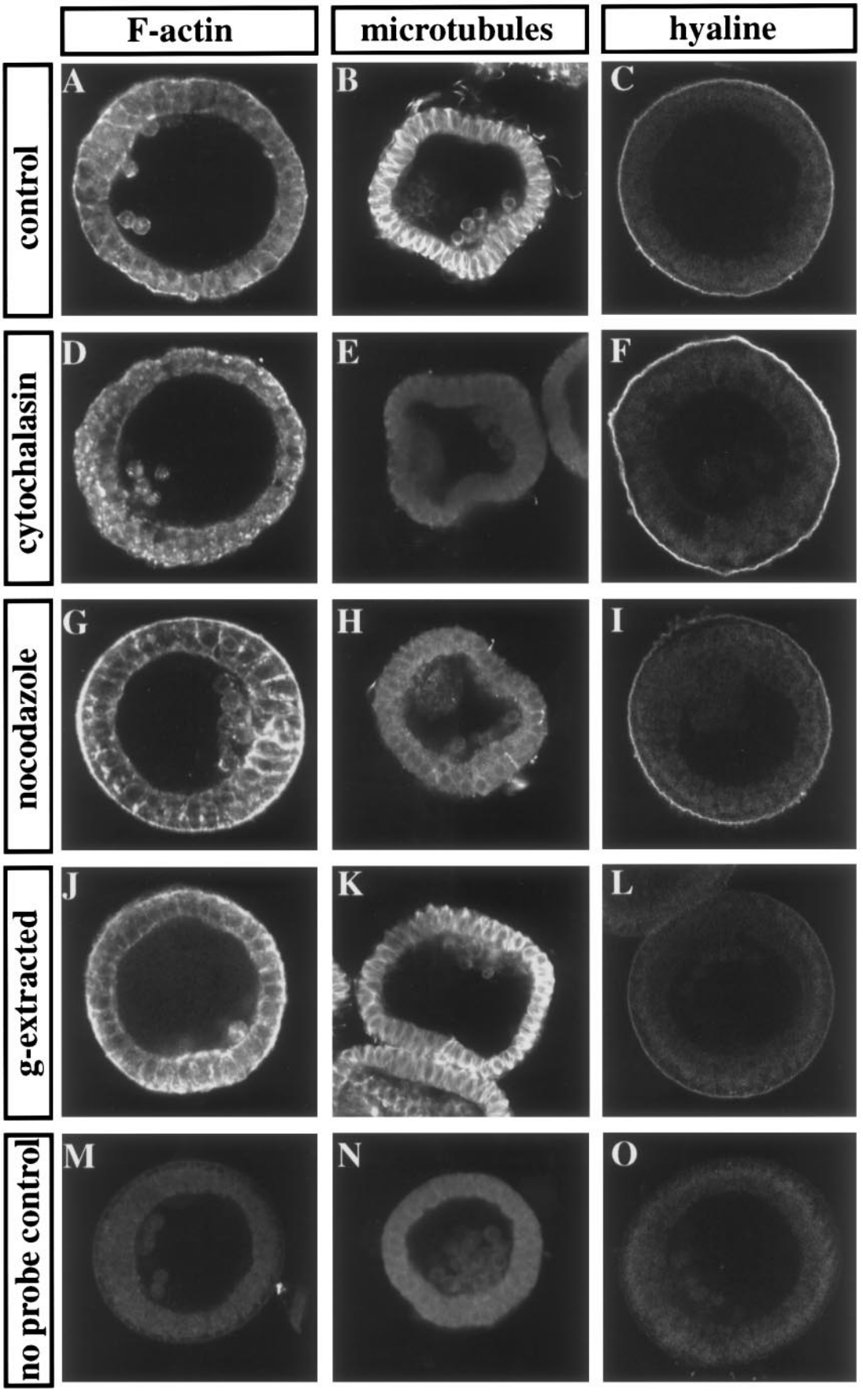
F-actin
microtubules
hyaline
control
cytochalasin
nocodazole
g-extracted
no probe control
A
B
C
D
E
F
G
H
I
J
K
L
M
N
O

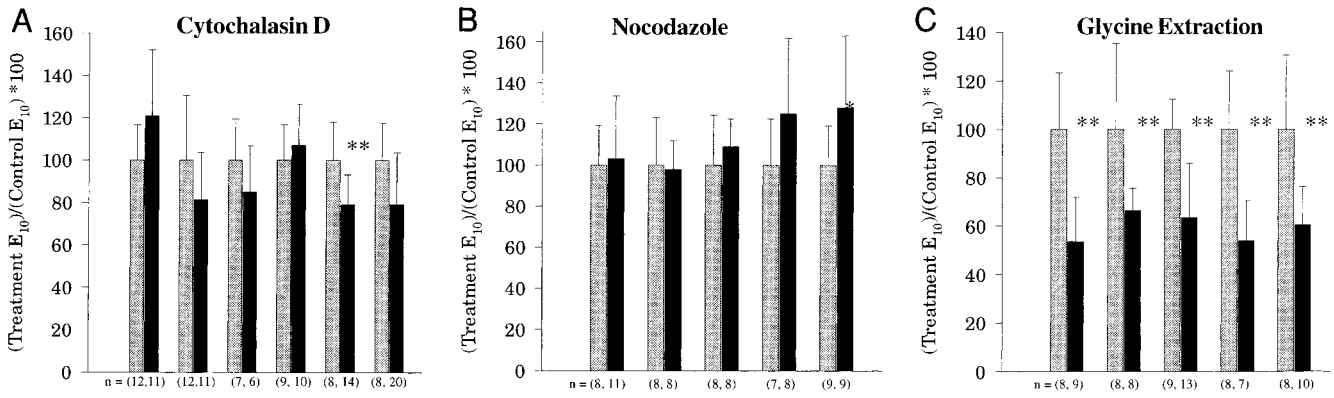

FIG. 5. Effects of cytochalasin D, nocodazole, and glycine extraction on E_{10} in *S. purpuratus* embryos from mesenchyme blastula stages. A single asterisk indicates that the treatment differed significantly ($P < 0.05$) from the control, while two asterisks indicate a highly significant difference ($P < 0.01$) as determined by the Mann–Whitney U test. The controls are represented by the gray bars while the experimental treatments are represented by black bars. (A) Ratio of the mean E_{10} of the blastocoel wall of embryos incubated with 6 μM cytochalasin D treatment for less than 60 min to the E_{10} of the blastula wall from untreated embryos for six cultures. (B) Ratio of the mean E_{10} of the blastocoel wall of embryos incubated with 40 μM nocodazole treatment to the E_{10} of the blastocoel wall from untreated embryos for five cultures. (C) Ratio of the mean E_{10} of the blastula wall of embryos extracted with glycine to the E_{10} of the blastula wall from untreated embryos for five cultures. (Error bars indicate 1 SD.)

Mechanical Consequences of Disrupting the Cytoskeleton and Apical ECM

To determine the role of the cell layer in the material properties of the blastula wall, cultures were treated with either cytochalasin D or nocodazole to disrupt the actin-based or microtubule-based cytoskeleton responsible for the mechanical properties of the epithelial cell layer (Janmey, 1991).

We determined the effect of each inhibitor on the distribution of F-actin, microtubules, and the apical extracellular matrix protein hyalin (see Fig. 4). As expected, cytochalasin D completely disrupted the F-actin array, reducing the subcortical localization (Fig. 4A) to a punctate pattern (Fig. 4D). While cytochalasin D had no effect on the distribution of hyalin protein (compare Fig. 4C to Fig. 4F), it proved to be effective at disrupting the paraxial microtubule arrays seen in controls (compare Fig. 4B to 4E). Nocodazole completely disrupted the paraxial microtubule arrays (Fig. 4H) seen in control embryos (Fig. 4B), but had no effect on either the hyalin protein (Fig. 4I) or F-actin (Fig. 4G). Glycine extraction reduced, but did not eliminate, the hyalin protein distribution in the apical ECM (compare Fig. 4C to 4L). Glycine extraction had no effect on the distribution of F-actin or microtubules (Figs. 4J and 4K). With the exception of cytochalasin D, each of our treatments was effective at disrupting their specific targets.

We then determined the effect of each of these treatments on the stiffness of the blastula wall. In six cultures incubated with cytochalasin D to disrupt F-actin for up to 60 min, there was no significant effect on the E_{10} (56 control and 72 cytochalasin D-treated embryos from six cultures; $P = 0.12$ by two-way ANOVA; Fig. 5A). Furthermore, there was no significant effect on the E_{10} from five cultures treated with nocodazole to disrupt the microtubule-based cytoskeleton (40 control and 44 nocodazole-treated embryos from five cultures; $P = 0.0975$ by two-way ANOVA; Fig. 5B). Thus, the major contributors to the stiffness of the cell layer, i.e., the F-actin and microtubules, contribute little if anything to the composite stiffness of the blastula wall.

If the stiffness of the composite does not lie in the cell layer, it must reside in the ECM. To determine the role of the apical ECM in the material properties of the embryo, five cultures were gently extracted with glycine and subjected to compression tests. In all five cultures the E_{10} was reduced between 40 and 50% (41 control and 47 glycine-extracted embryos from five cultures; $P < 0.0001$ by two-way ANOVA; Fig. 5C). Thus, the apical ECM is a major contributor to the stiffness of the blastula wall.

Long-Term Cytochalasin D Treatment

After incubating blastula stage sea urchin embryos for more than 60 min in cytochalasin D, the E_{10} suffered a significant decrease in four of the seven cultures tested (60 controls and 63 embryos treated with cytochalasin D; $P < 0.0001$ by two-way ANOVA); for a single culture, incubated for longer than 90 min, the forces resisting compression were too low to be measured. Accompanying this apparent loss of stiffness, gaps between cells in the epithelium were observed and delamination of the ECM from the apical cellular surface occurred. Since the mathematical model we used to calculate the stiffness of the blastula wall assumes that the volume of fluid in the blastocoel remains constant while an embryo is compressed, the stiffness determined

from embryos after long incubation in cytochalasin D does not represent the composite stiffness of the blastula wall.

Leakiness of the Blastocoel Wall

The mathematical model we used to calculate the stiffness of the blastula wall assumes that the volume of fluid in the blastocoel remains constant throughout the compression test. Leakage of fluid from the embryo's blastocoel could mimic the decrease in embryo stiffness seen over the course of compression. The magnitude of this effect can be illustrated by the following hypothetical case. Immediately after the initial compression, the microneedle is displaced by 14 μm. After compression, 20% of the volume begins to leak out of the embryo. As the compressed embryo's volume decreases, the diameter of the embryo decreases by 7%, allowing the microneedle to displace the compressed embryo by an additional 7 μm. Thus, in our hypothetical case, flow of fluid out of the embryo reduces the displacement of the microneedle from 14 to 7 μm, thus reducing the applied force and the calculated stiffness by 50%. After extended treatment with cytochalasin D, the epithelium can develop large holes, but we also needed to evaluate the permeability of small molecules such as water that could leak out through less obvious lesions in the epithelium.

Since we could not track the flow of water directly, we tested the permeability of the embryo's blastula wall by measuring the volume of embryos over the course of compression. As with the stiffness, we focused on the volume change in the first 10 s of compression (Table 2). For completeness, we included those embryos that were compressed after deciliation with hypotonic seawater (see Materials and Methods).

Our first question was whether control embryos changed volume after compression. To answer this we combined control and deciliated embryos into a single group and determined that embryos lost 1.2% (±7.9%) of their initial volume after 10 s of compression. This volume loss was very small but statistically significant ($P = 0.017$, paired-samples t test; $n = 244$; note: the number of control embryos does not equal the sum of the controls and deciliated from Table 2 since some control embryos were used for both long- and short-duration cytochalasin D treatments and were thus included only once in this large combined control group). We analyzed volume loss from 10 to 120 s and found that there was a significant additional volume loss of 0.6% ($P = 0.004$, paired-samples t test; $n = 244$). Thus, while there is some volume loss, 1.8% over the course of compression, it cannot account for time-dependent changes seen in the stiffness.

Our next question was whether embryos subjected to specific treatments were more leaky than the corresponding control embryos after being compressed. Again, to answer this question we looked at whether the percentage volume change for each treatment differed from the percentage volume change observed in the controls. Glycine-extracted embryos showed no significant effect on percentage volume lost after either 10 s ($P = 0.60$, two-way ANOVA) or from 10 to 120 s ($P = 0.88$, two-way ANOVA). Similarly, nocodazole treatment showed no significant effect on percentage volume lost after 10 s ($P = 0.67$, two-way ANOVA). However, short-duration cytochalasin D treatment demonstrated significant effects on the percentage volume lost as embryos incubated for 0 to 60 min lost 3.6% (±6.7%) of their initial volume after 10 s of compression ($P = 0.003$, two-way ANOVA). Long-duration cytochalasin D treatment also demonstrated significant effects on the percentage volume lost as embryos incubated more than 60 min lost 4.3% (±7.4%) of their initial volume after 10 s of compression ($P < 0.0001$, two-way ANOVA). Of all the treatments, only cytochalasin D allowed significant volume loss over the course of compression. Thus, volume loss might explain the decreased stiffness seen in embryos treated with cytochalasin D for more than 60 min but cannot explain the decreased stiffness of glycine-extracted embryos.

Effect of Glycine Extraction on Initial Volume

Embryos that had been glycine extracted were smaller than controls (volume decreased by 21%; $P < 0.0001$, two-way ANOVA). We do not understand how glycine extraction shrinks embryos; however, one possibility concerned us. The change in volume might reflect a change in the initial strain of the glycine-extracted embryos. Since our mathematical model for the calculation of the stiffness assumes a constant initial strain (see Appendix), a decrease could generate an artificially low measurement of the stiffness. To determine the magnitude of this potential source of error, we set about to determine whether glycine-extracted embryos were in effect "deflated." The most direct method we chose was to puncture embryos and measure changes in their circumference. Embryos with differing degrees of "inflation" could be expected to deflate differently when punctured. We measured changes in the circumference of embryos from 10 to 120 s after piercing and found no significant differences between the deflation of 18 control embryos and 29 glycine-extracted embryos from three cultures ($P = 0.65$, two-way ANOVA). Thus, the reduced stiffness of the blastula wall of glycine-extracted embryos reflects an intrinsic change in the stiffness rather than a change in the initial strain of the blastula wall.

CONCLUSIONS

Epithelial bending is an important physical process driving morphogenesis in animals. Sea urchin primary invagination has been an exceptionally useful system to study basic features of these movements. A number of hypotheses for mechanisms underlying primary invagination have been proposed in recent years. Our computer simulations (Davidson *et al.*, 1995) have confirmed that it is physically possible to generate a pit in the vegetal plate of a blastula by each of the following mechanisms: cells tractoring toward

TABLE 1
Time-Dependent Stiffness and Viscoelastic Model Parameters of *S. purpuratus* Blastocoel Wall of Control and Treated Embryos

Culture	Treatment	*n*	E_{10} (Pa) (± SD)	k_1 (Pa)	k_2 (Pa)	μ (Pa*s)
1	Control	12	1470 (250)	500	1200	49,000
	Cyto D	11	1780 (460)	620	1400	70,000
2	Control	12	2120 (650)	760	1800	65,400
	Cyto D	11	1730 (480)	440	1600	75,000
3	Control	7	2270 (450)	900	1700	76,000
	Cyto D	6	1940 (500)	1300	1200	21,000
4	Control	9	1110 (190)	450	850	33,000
	Cyto D	10	1180 (220)	520	910	29,000
5	Control	8	820 (150)	250	740	27,000
	Cyto D	14	650 (120)	220	610	17,000
6	Control	8	890 (160)	350	730	24,000
	Cyto D	20	700 (220)	240	610	22,000
1	Control	8	1870 (360)	1100	930	43,000
	Nocod	11	1930 (570)	1200	820	54,000
2	Control	8	1350 (310)	730	820	28,000
	Nocod	8	1330 (190)	640	810	47,000
3	Control	8	590 (140)	280	440	12,000
	Nocod	8	640 (80)	250	490	22,000
4	Control	7	1030 (230)	460	810	24,000
	Nocod	8	1290 (380)	530	1200	26,000
5	Control	9	830 (150)	420	580	17,000
	Nocod	9	1060 (290)	530	900	17,000
1	Control	8	630 (150)	290	410	21,000
	Glycine ext	9	340 (120)	210	170	4,900
2	Control	8	880 (310)	400	630	22,000
	Glycine ext	8	580 (80)	180	440	44,000
3	Control	9	1120 (140)	420	930	33,000
	Glycine ext	13	710 (250)	370	470	14,000
4	Control	8	1450 (350)	400	1400	53,000
	Glycine ext	7	780 (240)	420	460	18,000
5	Control	8	960 (120)	490	670	19,000
	Glycine ext	10	580 (150)	340	370	8,800

the center of the vegetal plate, apical constriction of cells in the vegetal plate, apical contraction by a ring of cells surrounding the vegetal plate, apicobasal contraction of cells in the vegetal plate, and gel swelling in the apical ECM of the vegetal plate. However, these computer models also revealed that each of these mechanisms operates within limited regimes of mechanical properties of the blastula wall (Davidson *et al.*, 1995). Cell tractoring, gel swelling, and apicobasal contraction mechanisms require that the apical ECM be stiffer than the cells to create an invagination; in contrast, apical constriction and apical ring contraction mechanisms require the apical ECM be of similar or lower stiffness than the cells. Thus, an embryo's mechanical design places physical constraints on the effectiveness of different force-generating processes driving invagination. In this paper we have measured the stiffness of the blastula wall in sea urchin embryos at mesenchyme blastula stages and have begun to assess the relative stiffness of the cell and apical ECM layers that determine which mechanisms of primary invagination are physically plausible.

The Blastula Wall Is Viscoelastic

The decrease in stiffness during our compression test indicates that the sea urchin's blastula wall responds to tension as a viscoelastic material. Table 1 summarizes the results of all experiments, listing the mean time-dependent stiffness of the tissues, as well as the spring constants and the coefficient of viscosity calculated for the standard material model of a viscoelastic material described in the legend to Fig. 2A. Compared with the stiffness properties of other biological materials listed in Table 2, the sea urchin blastula wall exhibits an initial stiffness ($[k_1 + k_2]$ ranging from 700 to 2600 Pa) that is considerably lower than that of complex basement membranes like the bovine retina (Table 2). Even after long-term application of the load, the stiffness of the sea urchin embryo tissues (k_2 ranges from 410 to 1800 Pa) remains greater than gels made of purified cytoskeletal components like actin, microtubules, and vimentin (Table 2). These results are consistent with a single reported measurement of 450 Pa for the stiffness of the blastula wall

TABLE 2
Stiffness of Cells and Tissues

Material	Stiffness (kPa)	Source	Technique used to determine
Actin (single filament)	2,600,000	(Gittes *et al.*, 1993)	Video analysis of thermal fluctuations in shape.
Microtubule (single filament)	1,200,000	(Gittes *et al.*, 1993)	Video analysis of thermal fluctuations in shape.
Lens capsule (basement membrane)	820	(Fisher and Wakely, 1976)	Distension chamber. Deformation of an edge-clamped circular membrane under pressure.
Chick DRG neurite axon	440	(Bray, 1979; Dennerll *et al.*, 1989)[a]	Calibrated glass needle and video displacement.
Type 1 collagen lattice	100	(Chapuis and Agache, 1992)	Stretched lattice rings using an instron.
Isolated bovine retina	20	(Jones *et al.*, 1992)	Deformation of an edge-clamped circular membrane with central point loading. Video analysis of deformation and force transducer determination of central load.
Physarum cytoplasmic strands	<10 to 30	(Adams, 1992)	Transducer and piezo positioner.
Sea anenome mesoglea	10	(Gosline, 1971)	Transducer and positioner.
Embryonic chick tissues		(Foty *et al.*, 1994)[b]	Transducer and video displacements.
Liver	4		
Heart	8		
Red blood cell cortex	3	(Hochmuth, 1993; Skalak *et al.*, 1973)	Micropipet-based pressure probe.
Xenopus notochord cells	0.9	(Koehl *et al.*, 1990)[c]	Glass fiber, video displacement, and three-point bending.
MDCK epithelial cell domes	0.64	(Tanner *et al.*, 1983)	Pressure measurements and shape analysis using thin membrane analysis.
Blood clot	0.6	(Jen and McIntire, 1982)	Parallel plate rheometer.
Blastula wall of *Psammechinus miliaris*	0.45	(Gustafson and Wolpert, 1963)	"Cell elastimeter" (Mitchison and Swann, 1954)
Cochlear hair cells	0.3	(Holley and Ashmore, 1988)[d]	Calibrated glass needles.
Actin	0.3	(Janmey *et al.*, 1991)	Parallel plate rheometer.
Fibrin	0.1		Measurements made on gels.
Microtubule	0.030		
Vimentin	0.030		
Sea urchin egg cortex	0.120 to 0.4	(Hiramoto, 1963)	Calibrated glass needle.
Cultured porcine aortic endothelial cells	0.115 to 0.14	(Sato *et al.*, 1990)	Micropipet-based pressure probe and video analysis.
Human leukocytes	0.010 to 0.1	(Hochmuth, 1993; Schmid-Schonbein *et al.*, 1981; Sung *et al.*, 1988)	Micropipet-based pressure probe and video analysis.
Actin and α-actinin (based on deformation frequency)	0.010 to 1.0	(Sato *et al.*, 1987)	Cone and plate rheometer.
Actin and gelsolin	0.1	(Janmey *et al.*, 1988)	Parallel plate rheometer.
Tracheal mucus	0.062	(Seybold *et al.*, 1990)	Double capillary rheometer.
Xenopus IMZ explants	0.007 to 0.014	(Moore *et al.*, 1995)	Calibrated optical fiber with computer control.

[a] Estimated from spring stiffness measured by Dennerll *et al.* (1988) and the cross-sectional area of DRG neurons measured by Bray (1979).
[b] Estimated from the surface tension and an approximate thickness of the enveloping cell layer of 50 μm.
[c] Estimated from the flexural stiffness of the notochord when the sheath is deflated (assumed all stiffness due to cells).
[d] Estimate based on an assumption that the cochlear hair cell is a homogeneous elastic solid.

of another sea urchin species, *Psammechinus miliaris* (Gustafson and Wolpert, 1963).

The coefficient of viscosity (μ) of the blastula wall (see Table 1) ranged from 12,000 to 76,000 Pa · s. Viscosity is a measure of the relation between the magnitude of the applied stress and the rate of change in strain in the tissue.

Consider a material loaded with an applied stress: if the strain changes quickly the coefficient is small. For comparison, glycerine at room temperature has a coefficient of viscosity of 0.3 Pa · s while the viscosity of water is about 10^{-3} Pa · s (White, 1991). Compared with published values of viscosity of various types of cytoplasm and cellular components listed in Table 1 of Bereiter-Hahn (1987; viscosities ranged from 0 to 1000 Pa · s), the blastula wall (composed of the cell layer and apical ECM) of the mesenchyme blastula has an exceptionally high viscosity. Only pulmonary macrophages (with a viscosity of 120,000 to 270,000 Pa · s) and "living" squid axoplasm (with a viscosity of 10^6 to 10^7 Pa · s) are higher than that of the blastula wall (Sato *et al.,* 1984).

The Blastula Wall Derives Little of Its Composite Stiffness from the Actin or Microtubule Cytoskeleton

The lack of any immediate effect of either nocodazole or cytochalasin D on the stiffness of the blastula wall indicates that its bulk mechanical properties are not due to the microtubule or actin cytoskeleton but rather are derived from the stiffness of either intermediate filaments in the cells or the apical ECM. While sea urchin embryos possess intermediate filaments (Boyle and Ernst, 1989), similar intermediate filament networks in *Xenopus* embryos are sensitive to disruption by both nocodazole and cytochalasin (Gard *et al.,* 1997). Thus, we suggest that the ECM is responsible for the stiffness of the blastula wall based on our measurements of reduced stiffness of glycine-extracted embryos and on our calculations that the cell layer contributes little to the overall stiffness of the blastula wall (see Appendix). We have identified 700 Pa as the upper limit to the cell stiffness (i.e., the E_{10} of the cell layer alone) and we have calculated 4100 Pa to be the lower limit of the stiffness of the apical ECM.

If the Extracellular Matrix Is Stiffer Than the Cells, Then Neither Apical Constriction nor Annular Ring Contraction Can Generate an Invagination

We can now narrow the field of hypotheses of primary invagination in *S. purpuratus* to those that remain physically plausible. Combining our measurements of stiffness with the predictions of computer simulations (Davidson *et al.,* 1995), we can rate the effectiveness of each mechanism to drive invagination. As demonstrated by the computer simulations, each model's effectiveness hinges on the relative stiffness properties of the cell layer and apical ECM. Figure 6 illustrates a possible range of material properties measured here for mesenchyme blastula stage embryos compared with the predicted effectiveness of five different models of primary invagination [see Fig. 9 in Davidson *et al.* (1995)]. We previously found that the apical constriction hypothesis and the annular ring contraction model required the apical ECM be of similar or lower stiffness than the cells. This study indicates that neither the actin-based nor the microtubule-based cytoskeleton makes a contribution to the composite stiffness of the blastula wall and that the apical ECM is much stiffer than the cell layer. Thus, based on these findings on the mechanical design of the blastula, the apical constriction and apical ring contraction mechanisms do not appear to be physically plausible engines for invagination in this species.

F-Actin, Apical Constriction, and Bottle Cells

Apical constriction continues to be one of the more commonly cited mechanisms for driving epithelial bending [e.g., chick neurulation (Schoenwolf *et al.,* 1988); *Drosophila* ventral furrow formation (Costa *et al.,* 1994)]. Several groups have suggested that primary invagination in the sea urchin is driven by the apical constriction of a ring of bottle cells surrounding the vegetal plate (Kimberly and Hardin, 1998; Nakajima and Burke, 1996). Nakakima and Burke proposed that an F-actin network at the apical end of cells in the vegetal plate contract, driven by myosin, such that the apical surface of the archenteron decreases. A vegetal plate bending force is generated as cytoplasm is pushed toward the basal surface of the vegetal plate. Thus, bottle cells are created at the same time that the vegetal plate bends inward during the initial movements of invagination. As in other instances of epithelial bending, the apical contraction hypothesis finds support in the localization of F-actin at the apical face of bottle cells and the absence of localized F-actin when invagination is blocked experimentally in *S. purpuratus* embryos (Nakajima and Burke, 1996). Using 4-D Nomarski microscopy to identify and a laser to ablate various groups of cells in the vegetal plate, Kimberly and Hardin (1998) showed that bottle cells form as the archenteron deepens and that they alone are required to drive invagination in *Lytechinus pictus* embryos. Since laser ablation is damaging to both the bottle cells and the underlying apical ECM (cellular debris is extruded through the apical extracellular matrix), it is unclear whether invagination is driven by apical shape changes in the bottle cells or some other function of these cells.

While an intact group of bottle cells appears essential for the initial movements of invagination, the function of apically localized F-actin and its role in apical constriction are debatable (see Davidson *et al.,* 1995). One alternative explanation for the accumulation of actin into the apical face of the vegetal plate might be extrapolated from recent work on cultured cells subjected to applied stress (Glogauer *et al.,* 1998). These studies have found that cells subjected to increased mechanical stress through cadherin-mediated junctions recruit more F-actin into their respective junctions. Thus, the increase in actin label in the vegetal plate may simply indicate a region of high mechanical stress. An example of F-actin localization that might correlate with high stress can be seen in the apical face of ingressing primary mesenchyme cells in *L. pictus* (Anstrom, 1992; Anstrom and Raff, 1988); these bottle-shaped cells exhibit intense actin localization in their trailing apical "foot" yet do not generate an invagination in the vegetal plate.

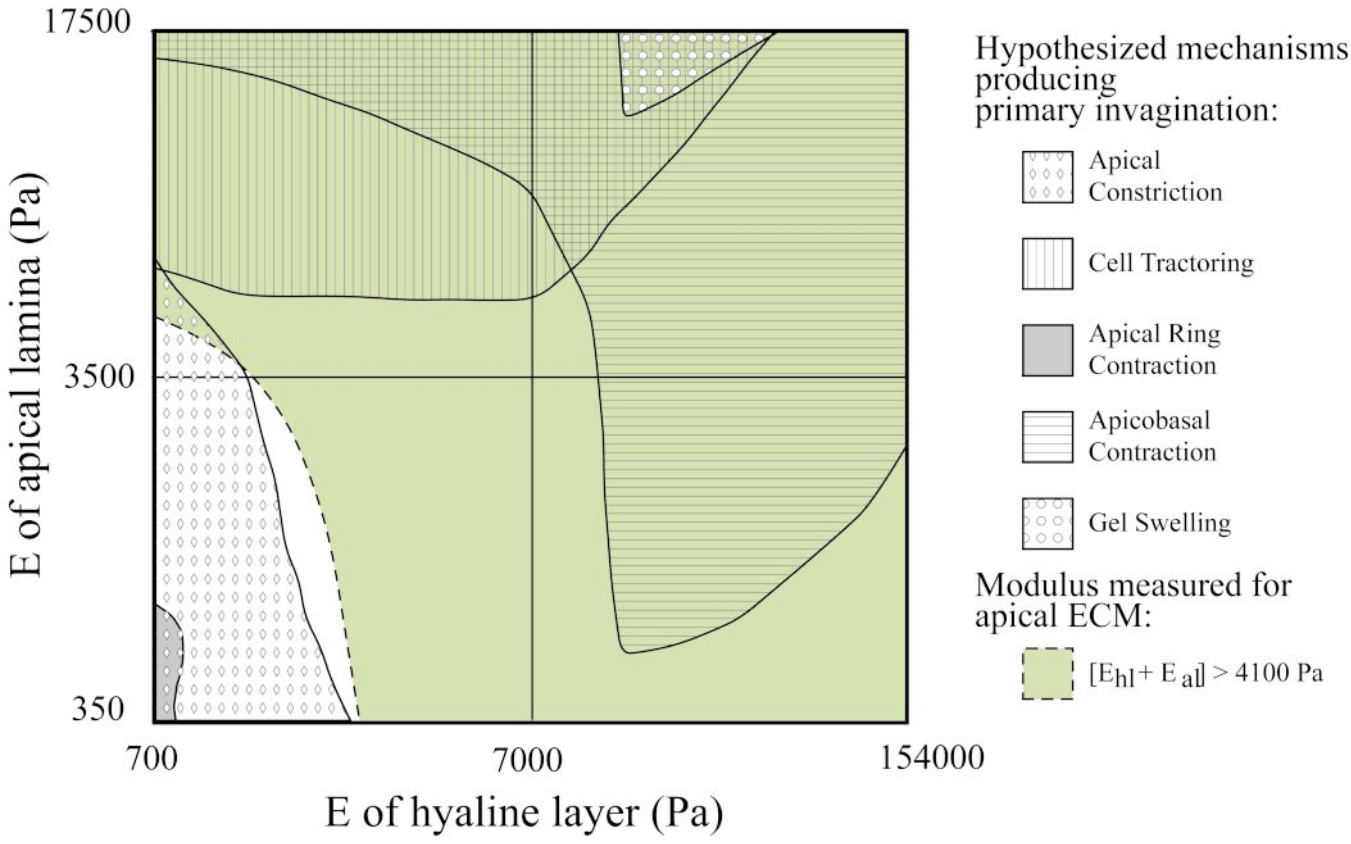

FIG. 6. Material properties predicted in Davidson *et al.* (1995) and the range of mechanical properties of the blastula wall as determined by compression tests. The material parameter space shows regions occupied by the five models. The cell layer stiffness is 700 Pa. The shaded regions indicate regions of the stiffness parameter space wherein each of five hypotheses is capable of generating invaginations greater than 12 μm. The green-filled region indicates the region of the parameter space occupied by the tissue mechanical properties of the *S. purpuratus* embryos measured here. Note that while the scale of stiffness changes in each quadrant, the material properties are continuous.

Thus, any treatment that prevents the generation of force or the transmission of that force to the cell might also inhibit the stress-induced accumulation of F-actin. Clearly, these speculative digressions on the role of F-actin during primary invagination highlight a critical gap in our understanding of the mechanics of epithelial bending.

Apicobasal Contraction of Bottle Cells Could Drive Invagination

Apicobasal contraction of a ring of bottle cells already present in the vegetal plate at the onset of invagination could drive invagination within the context of a relatively stiff apical extracellular matrix. Cells of the vegetal plate columnarize and produce a population of bottle cells with contracted apices in the vegetal plate prior to invagination in *L. pictus* embryos (Ettensohn, 1984b; Kimberly and Hardin, 1998). The capacity of these cells to generate an invagination with additional apical constriction is limited since these bottle cells are already contracted. However, these cells still have a mechanical advantage and may bend the vegetal plate inward by contracting in the apicobasal direction (see the apicobasal contraction hypothesis in Davidson *et al.*, 1995). Some support for this proposal can be found in the only report of changes in cell height in the vegetal plate (Ettensohn, 1984b) where average cell heights throughout the vegetal plate in *L. pictus* embryos decreased by 11% over the course of invagination. Whether bottle cells change height as the flat vegetal plate begins to bend inward is unknown.

Biomechanics and the Morphogenetic Mechanism Driving Primary Invagination

With this and our previous paper (Davidson *et al.*, 1995), we have conducted a biomechanical analysis (Koehl, 1990) of sea urchin primary invagination: (i) we have quantified shape changes during primary invagination (Davidson,

1995), (ii) we have formulated physical theories about the different hypothesized driving forces and used computer models to identify the parameter space in which each mechanism can drive primary invagination (Davidson *et al.*, 1995), and (iii) we have empirically determined those parameters. We have measured the stiffness of the blastula wall of the sea urchin and have used cytochalasin D, nocodazole, and glycine extraction to determine the relative contribution of the cell and ECM layers to that stiffness. We found that the apical ECM is considerably stiffer than the cell layer. These measurements, when combined with previous modeling results, show that neither apical constriction nor annular ring contraction hypotheses can drive invagination. If, as we suggest, the apical ECM is much stiffer than the cell layer in the blastula wall, then each of the other three hypothesized mechanisms, cell tractoring, gel swelling, and apicobasal contraction, is capable of driving invagination. These remaining hypothesized mechanisms of cell tractoring, gel swelling, and apicobasal contraction must now be tested.

Our approach in this paper establishes a framework to understand and test the mechanical roles of cells and tissues that are directly responsible for invagination. Our findings support important roles for the apical extracellular matrix as either a mechanical structure for apicobasal contraction, a force generating structure for gel swelling, or a substrate for cell tractoring. In addition to these mechanical roles, the apical ECM may support signaling and patterning functions required to establish the spatial and temporal boundaries of cell behaviors driving invagination.

APPENDIX: CALCULATION OF THE ELASTIC MODULUS (I.E., STIFFNESS) OF THE WALL TISSUE OF A COMPRESSED MESENCHYME BLASTULA

The sea urchin mesenchyme blastula can be thought of as a hydrostat. Hydrostats are characterized by two mechanically important features: an internal pressurized fluid and an elastic membrane under tension (e.g., Wainwright, 1988). In the blastula hydrostat, the cell layer and apical ECM combine to form a composite membrane under tension surrounding the pressurized, fluid-filled blastocoel. While an intact epithelium is not necessary for invagination to proceed (Ettensohn, 1984a; Moore and Burt, 1939), it is necessary in order to apply the compression technique to assay the stiffness properties of the composite blastula wall.

The time-dependent elastic modulus, $E(t)$, representing the composite stiffness of the sea urchin blastula wall, was determined at timed intervals using the deformed geometry of the compressed embryo. The derivation of that stiffness relies on a simple thin membrane representation of the embryo (Hiramoto, 1963).

In the whole embryo, the force equilibrium equation requires that forces within the plane of the membrane balance:

$$\frac{N_\theta}{R_1} + \frac{N_\varphi}{R_2} = P, \qquad [1]$$

where N_θ and N_φ are the tensions (force per unit length) in the direction of the equator and that in the direction of the meridian, respectively; R_1 and R_2 are corresponding principle radii of curvature as shown in Fig. 1C; and P is the initial internal pressure (force/area), that is, the pressure difference between the blastocoel and outside of the embryo, acting normal to the surface. This equation is similar to that used by Cole (1932) and Cole and Michaelis (1932) in their studies on *Arbacia* eggs as well as by Foty *et al.* (1994) to calculate surface tension of compressed tissue aggregates.

If the whole embryo is compressed between a mica sheet and a solid backing, then the force (F) applied to the embryo wall by the mica sheet balances the internal pressure (P) over the contact area (A) between the sheet and the embryo:

$$P = \frac{F}{A}. \qquad [2]$$

In the compressed embryo, the equation of the force equilibrium in the blastula wall at the equatorial plane is

$$2\pi R_1 N_\varphi + F = \pi R_1^2 P, \qquad [3]$$

where R_1 is defined in Fig. 1C.

Determination of the elastic modulus requires a description of the elastic response of the blastula wall to these forces at equilibrium. Consider a small piece of the wall of the embryo (with thickness h_0 before compression) from the equatorial region. This piece of the blastula wall in the pressurized embryo is under a tensile strain ϵ_0 acting in the plane, so that the length of the side of that piece is $\alpha(1 + \epsilon_0)$, where α is the length of the side of the piece in the resting state. Then in the compressed embryo, this piece is stretched so that the length along the meridian becomes $\alpha(1 + \epsilon_\varphi)$ and the length of the sides parallel to the equator changes to $\alpha(1 + \epsilon_\theta)$. Compression then generates tensile stresses (force per cross-sectional area) along the meridian (σ_φ) and equatorial (σ_θ) faces of the piece. The elastic modulus (E) of the piece then satisfies the following four equations:

$$\sigma_\varphi = N_\varphi \frac{(1 + \epsilon_\varphi)(1 + \epsilon_\theta)}{h} \qquad [4]$$

$$\sigma_\theta = N_\theta \frac{(1 + \epsilon_\varphi)(1 + \epsilon_\theta)}{h} \qquad [5]$$

$$\epsilon_\varphi = \frac{(\sigma_\varphi - 0.5\sigma_\theta)}{E} \qquad [6]$$

$$\epsilon_\theta = \frac{(\sigma_\theta - 0.5\sigma_\varphi)}{E}, \qquad [7]$$

where a value of 0.5 has been chosen for the Poisson's ratio

(a measure of the ability of a material to change volume and change shape; a ratio of 0.5 indicates that the material does not change volume, but can change shape easily) as well as the thickness (h) of the combined cell and apical ECM layers. Changes in the shape of this small piece of tissue can be related to the large-scale deformation of the whole embryo (R_1 and R_2 defined in Fig. 1C):

$$\frac{(1 + \epsilon_\theta)}{(1 + \epsilon_0)} = \frac{R_1}{R_2}. \quad [8]$$

Additionally, the thickness of the tissue without deformation (h_0), the thickness of the deformed tissue (h), and the initial strain in the plane of the tissue (ϵ_0) are related by

$$h_0 = \frac{h}{(1 + \epsilon_0)^2}. \quad [9]$$

Eliminating σ_θ, σ_ϕ, ϵ_θ, ϵ_ϕ, and h for Eqs. [5], [6], [7], [8], [9], and [10],

$$E\left[\frac{R_1}{R_0} - \frac{1}{1 + \epsilon_0}\right] = \frac{R_1}{(1 + \epsilon_0)^2 h_0 R_0}\left[1.5(N_\theta - N_\varphi) + \frac{R_1}{R_0}(1 + \epsilon_0)(N_\varphi - 0.5N_\theta)\right], \quad [10]$$

solving for the tensional forces,

$$N_\varphi = \frac{1}{2\pi R_1}(\pi R_1^2 P - F) \quad [11]$$

$$N_\theta = PR_1 - \frac{1}{2\pi R_2}(\pi R_1^2 P - F) \quad [12]$$

and substituting Eqs. [13] and [14] into Eq. [12] yield the modulus (E) in terms of the quantities h_0, ϵ_0, F, R_0, R_1, R_2, and R_c,

$$E = -\frac{1}{4} F \frac{\begin{array}{r} 3R_0R_1R_c^2 - 3R_0R_1^3 + 3R_0R_1^2R_2 + 3R_0R_2R_c^2 \\ - 2R_1R_2R_c^2 - R_1^2R_c^2 + R_1^4(1 + \epsilon_0) \\ - 2\epsilon_0R_1R_2R_c^2 - \epsilon_0R_1^2R_c^2 \end{array}}{\pi h_0 R_0 R_2 R_c^2 (R_0 - R_1(1 + \epsilon_0))(1 + \epsilon_0)}. \quad [13]$$

Modulii determined with Eq. [13] represent the composite modulus averaged over the whole surface of the embryo. By necessity, this analysis assumes that the structure and material properties are uniform over the whole embryo. Thus, the thickness of the uncompressed blastula wall (h_0) represents the thickness of the cell and apical ECM layers averaged over the whole embryo; a constant value of 10 μm was used throughout all the analyses. Similarly, the initial strain (ϵ_0) is also an averaged feature of the uncompressed blastula wall; a single value of 10% was used throughout all the analyses. However, the impact of the assumptions of the initial thickness and initial strain is minimal when actual values for the geometric parameters (R_0, R_1, R_2, and R_c) are substituted into Eq. [13].

Separating the Layer Modulii from the Composite Modulus

The elastic modulus (E) calculated from Eq. [13] is a composite modulus representing the contribution of the various materials that make up the complex layers of the wall of the embryo. A simple multilayered composite has a modulus that is the product of the modulus of its component layers (Christensen, 1991),

$$E_{\text{control}} = \frac{1}{h}(E_{\text{cell}}h_{\text{cell}} + E_{\text{al}}h_{\text{al}} + E_{\text{hl}}h_{\text{hl}}), \quad [14]$$

where the cell thickness (h_{cell}) and modulus (E_{cell}), apical lamina thickness (h_{al}) and modulus (E_{al}), and hyaline layer thickness (h_{hl}) and modulus (E_{hl}) each contribute to the composite modulus of the whole tissue (E_{control}) with a thickness (h).

After gentle glycine extraction, the ECM layer is reduced in either stiffness or thickness. If it were completely removed, the term [$E_{\text{al}} \cdot h_{\text{al}} + E_{\text{hl}} \cdot h_{\text{hl}}$] would be reduced to zero. Conservatively, then the composite stiffness of the blastula wall measured after glycine extraction reflects only the remaining cell layer terms [$E_{\text{cell}} \cdot h_{\text{cell}}$],

$$E_{\text{GGE}} = \frac{1}{h}(E_{\text{cell}}h_{\text{cell}} + 0 + 0), \quad [15]$$

where E_{GGE} refers to the modulus measured for embryos treated with gentle glycine extraction. Therefore, the modulus of the cell layer is

$$E_{\text{cell}} = \frac{h}{h_{\text{cell}}} E_{\text{GGE}}. \quad [16]$$

Substituting the E_{10} measured from control and glycine-extracted embryos for (E_{control}) and (E_{GGE}) in Eq. [16] and assuming that the thicknesses of the total blastula wall and cell layer are 10 and 9 μm [i.e., that the thickness of the apical ECM is approximately 1 μm (Spiegel *et al.*, 1989)], respectively, we find that E_{cell} after 10 s of compression ranged from 370 to 860 Pa for the five cultures subjected to gentle glycine extraction. We can then calculate the lowest possible stiffness of the ECM layers:

$$E_{\text{al}} + E_{\text{al}} = \frac{h}{h_{\text{ecm}}}(E_{\text{control}} - E_{\text{GGE}}). \quad [17]$$

We can then calculate the stiffness of the ECM layers assuming the total thickness of the blastula wall (h) and thickness of the ECM layer (h_{ecm}) are 10 and 1 μm, respectively; we find that E_{ecm} after 10 s of compression ranged

from 2900 to 4100 Pa for the five cultures subjected to gentle glycine extraction. Conservatively, these are the lowest values for the combined stiffness of the apical ECM composite.

ACKNOWLEDGMENTS

This research was supported by grants from NSF to M.K. and R.K. (92-20525), from NIH to R.K. (HD 25594), from NSF to G.O. (92-20719), and from NIH to L.D. (5T32GM07379). The authors thank Fred Wilt and Connie Lane for their considerable assistance and expert knowledge of gastrulation.

REFERENCES

Adams, D. S. (1992). Mechanisms of cell shape change: The cytomechanics of cellular response to chemical environment and mechanical loading. *J. Cell Biol.* **117,** 83–93.

Alliegro, M. C., Black, S. D., and McClay, D. R. (1992). Deployment of extracellular matrix proteins in sea urchin embryogenesis. *Microsc. Res. Tech.* **22,** 2–10.

Alliegro, M. C., and McClay, D. R. (1988). Storage and mobilization of extracellular matrix proteins during sea urchin development. *Dev. Biol.* **125,** 208–216.

Amemiya, S. (1989). Electron microscopic studies on primary mesenchyme cell ingression and gastrulation in relation to vegetal pole cell behavior in sea urchin embryos. *Exp. Cell Res.* **183,** 453–462.

Anstrom, J. A. (1992). Microfilaments, cell shape changes, and the formation of the primary mesenchyme in sea urchin embryos. *J. Exp. Zool.* **264,** 312–322.

Anstrom, J. A., and Raff, R. A. (1988). Sea urchin primary mesenchyme cells: Relation of cell polarity to the epithelial–mesenchymal transformation. *Dev. Biol.* **130,** 57–66.

Bereiter-Hahn, J. (1987). Mechanical principles of architecture of eukaryotic cells. *In* "Cytomechanics: The Mechanical Basis of Cell Form and Structure" (J. Bereiter-Hahn, O. R. Anderson, and W.-E. Reif, Eds.), pp. 3–30. Springer-Verlag, Berlin.

Boyle, J. A., and Ernst, S. G. (1989). Sea urchin oocytes possess elaborate cortical arrays of microfilaments, microtubules, and intermediate filaments. *Dev. Biol.* **134,** 72–84.

Bray, D. (1979). Mechanical tension produced by nerve cells in tissue culture. *J. Cell Sci.* **37,** 391–410.

Burke, R. D., Myers, R. L., Sexton, T. L., and Jackson, C. (1991). Cell movements during the initial phase of gastrulation in the sea urchin embryo. *Dev. Biol.* **146,** 542–557.

Burke, R. D., and Tamboline, C. R. (1990). Ontogeny of an extracellular matrix component of sea urchins and its role in morphogenesis. *Dev. Growth Diff.* **32,** 461–471.

Butler, E., Hardin, J., and Benson, S. (1987). The role of lysyl oxidase and collagen crosslinking during sea urchin development. *Exp. Cell Res.* **173,** 174–182.

Chapuis, J. F., and Agache, P. (1992). A new technique to study the mechanical properties of collagen lattices. *J. Biomech.* **25,** 115–120.

Christensen, R. M. (1991). "Mechanics of Composite Materials." Krieger, Malabar, FL.

Cole, K. S. (1932). Surface forces of the *Arbacia* egg. *J. Cell. Comp. Physiol.* **1,** 1–9.

Cole, K. S., and Michaelis, E. M. (1932). Surface forces of fertilized *Arbacia* eggs. *J. Cell. Comp. Physiol.* **2,** 121–126.

Costa, M., Wilson, E. T., and Wieschaus, E. (1994). A putative cell signal encoded by the folded gastrulation gene coordinates cell shape changes during *Drosophila* gastrulation. *Cell* **76,** 1075–1089.

Davidson, L. A. (1995). "Biomechanics of Sea Urchin Primary Invagination," Ph.D. Thesis. Univ. California Berkeley.

Davidson, L. A., Koehl, M. A. R., Keller, R., and Oster, G. F. (1995). How do sea urchins invaginate? Using biomechanics to distinguish between mechanisms of primary invagination. *Development* **121,** 2005–2018.

Dennerll, T. J., Lamoureux, P., Buxbaum, R. E., and Heidemann, S. R. (1989). The cytomechanics of axonal elongation and retraction. *J. Cell Biol.* **109,** 3073–3083.

Dent, J. A., Polson, A. G., and Klymkowsky, M. W. (1989). A whole-mount immunocytochemical analysis of the expression of the intermediate filament protein vimentin in *Xenopus*. *Development* **105,** 61–74.

Ettensohn, C. A. (1984a). "An Analysis of Invagination during Sea Urchin Gastrulation," Ph.D. Thesis. Yale Univ.

Ettensohn, C. A. (1984b). Primary invagination of the vegetal plate during sea urchin gastrulation. *Am. Zool.* **24,** 571–588.

Ettensohn, C. A. (1985a). Gastrulation in the sea urchin embryo is accompanied by the rearrangement of invaginating epithelial cells. *Dev. Biol.* **112,** 383–390.

Ettensohn, C. A. (1985b). Mechanisms of epithelial invagination. *Q. Rev. Biol.* **60,** 289–307.

Findley, W. N., Lai, J. S., and Onaran, K. (1989). "Creep and Relaxation of Nonlinear Viscoelastic Materials." Dover, New York.

Fisher, R. F., and Wakely, J. (1976). The elastic constants and ultrastructural organization of a basement membrane. *Proc. R. Soc. London Ser. B* **193,** 335–358.

Foty, R. A., Forgacs, G., Pfleger, C. M., and Steinberg, M. S. (1994). Liquid properties of embryonic tissues: Measurement of interfacial tensions. *Phys. Rev. Lett.* **72,** 2298–2301.

Gard, D. L. (1991). Organization, nucleation, and acetylation of microtubules in *Xenopus laevis* oocytes: A study by confocal immunofluorescence microscopy. *Dev. Biol.* **143,** 346–362.

Gard, D. L., Cha, B. J., and King, E. (1997). The organization and animal–vegetal asymmetry of cytokeratin filaments in stage VI *Xenopus* oocytes is dependent upon F-actin and microtubules. *Dev. Biol.* **184,** 95–114.

Gittes, F., Mickey, B., Nettleton, J., and Howard, J. (1993). Flexural rigidity of microtubules and actin filaments measured from thermal fluctuations in shape. *J. Cell Biol.* **120,** 923–934.

Glogauer, M., Arora, P., Chou, D., Janmey, P. A., Downey, G. P., and McCulloch, C. A. (1998). The role of actin-binding protein 280 in integrin-dependent mechanoprotection. *J. Biol. Chem.* **273,** 1689–1698.

Gosline, J. M. (1971). Connective tissue mechanics of *Metridium senile* II. Visco-elastic properties and macromolecular model. *J. Exp. Biol.* **55,** 775–795.

Gustafson, T., and Wolpert, L. (1963). The cellular basis of morphogenesis and sea urchin development. *Int. Rev. Cytol.* **15,** 139–214.

Hardin, J. D. (1987). Archenteron elongation in the sea urchin embryo is a microtubule-independent process. *Dev. Biol.* **121,** 253–262.

Hardin, J. D., and Cheng, L. Y. (1986). The mechanisms and mechanics of archenteron elongation during sea urchin gastrulation. *Dev. Biol.* **115,** 490–501.

Hawkins, R. L., Fan, J., and Hille, M. B. (1995). Gastrulation in the sea urchin, *Stongylocentrotus purpuratus,* is disrupted by the small laminin peptides YIGSR and IKVAV. *Cell Adh. Commun.* **3,** 163–177.

Hiramoto, Y. (1963). Mechanical properties of sea urchin eggs. I. Surface force and elastic modulus of the cell membrane. *Exp. Cell Res.* **32,** 59.

Hiramoto, Y. (1990). Mechanical properties of the cortex before and during cleavage. *Ann. N.Y. Acad. Sci.* **582,** 22–30.

Hochmuth, R. M. (1993). Measuring the mechanical properties of individual human blood cells. *J. Biomech. Eng.* **115,** 515–519.

Holley, M. C., and Ashmore, J. F. (1988). A cytoskeletal spring in cochlear outer hair cells. *Nature* **335,** 635–637.

Janmey, P. A. (1991). Mechanical properties of cytoskeletal polymers. *Curr. Opin. Cell Biol.* **3,** 4–11.

Janmey, P. A., Euteneuer, U., Traub, P., and Schliwa, M. (1991). Viscoelastic properties of vimentin compared with other filamentous biopolymer networks. *J. Cell Biol.* **113,** 155–160.

Janmey, P. A., Hvidt, S., Peetermans, J., Lamb, J., Ferry, J. D., and Stossel, T. P. (1988). Viscoelasticity of F-actin and F-actin/gelsolin complexes. *Biochemistry* **27,** 8218–8227.

Jen, C. J., and McIntire, L. V. (1982). The structural properties and contractile force of a clot. *Cell Motil.* **2,** 445–455.

Jones, I. L., Warner, M., and Stevens, J. D. (1992). Mathematical modelling of the elastic properties of retina: A determination of Young's modulus. *Eye* **6,** 556–559.

Kane, R. E. (1973). Hyalin release during normal sea urchin development and its replacement after removal at fertilization. *Exp. Cell Res.* **81,** 301–311.

Kimberly, E. L., and Hardin, J. (1998). Bottle cells are required for the initiation of primary invagination in the sea urchin embryo. *Dev. Biol.* **204,** 235–250.

Koehl, M. A. R. (1990). Biomechanical approaches to morphogenesis. *Semin. Dev. Biol.* **1,** 367–378.

Koehl, M. A. R., Adams, D. S., and Keller, R. E. (1990). Mechanical development of the notochord in *Xenopus* early tail-bud embryos. *In* "Biomechanics of Active Movement and Deformation" (N. Akkas, Ed.), Vol. H 42, pp. 471–485. Springer-Verlag, Berlin, Heidelberg.

Lane, M. C., Koehl, M. A. R., Wilt, F., and Keller, R. (1993). A role for regulated secretion of apical extracellular matrix during epithelial invagination in the sea urchin. *Development* **117,** 1049–1060.

McClay, D. R., and Fink, R. D. (1982). Sea urchin hyalin: Appearance and function in development. *Dev. Biol.* **92,** 285–293.

Miller, J. R., Fraser, S. E., and McClay, D. (1995). Dynamics of thin filopodia during sea urchin gastrulation. *Development* **121,** 2501–2511.

Miller, J. R., and McClay, D. R. (1997a). Changes in the pattern of adherens junction-associated β-catenin accompany morphogenesis in the sea urchin embryo. *Dev. Biol.* **192,** 310–322.

Miller, J. R., and McClay, D. R. (1997b). Characterization of the role of cadherin in regulating cell adhesion during sea urchin development. *Dev. Biol.* **192,** 323–339.

Mitchison, J. M., and Swann, M. M. (1954). The mechanical properties of the cell surface. I. The cell elastimeter. *J. Exp. Biol.* **31,** 443–461.

Moore, A. R. (1941). On the mechanics of gastrulation in *Dendraster excentricus. J. Exp. Zool.* **87,** 101–111.

Moore, A. R., and Burt, A. S. (1939). On the locus and nature of the forces causing gastrulation in the embryos of *Dendraster excentricus. J. Exp. Zool.* **82,** 159–171.

Moore, S. W., Keller, R. E., and Koehl, M. A. R. (1995). The dorsal involuting marginal zone stiffens anisotropically during its convergent extension in the gastrula of *Xenopus leavis. Development* **121,** 3130–3140.

Nakajima, Y., and Burke, R. D. (1996). The initial phase of gastrulation in sea urchins is accompanied by the formation of bottle cells. *Dev. Biol.* **179,** 436–446.

Ramachandran, R. K., Seid, C. A., Lee, H., and Tomlinson, C. R. (1993). PDGF-bb and TGF-α rescue gastrulation, spiculogenesis, and lps1 expression in collagen-disrupted embryos of the sea urchin genus *Lytechinus. Mech. Dev.* **44,** 33–40.

Ramachandran, R. K., Wikramanayake, A. H., Uzman, J. A., Govindarajan, V., and Tomlinson, C. R. (1997). Disruption of gastrulation and oral–aboral ectoderm differentiation in the *Lytechinus pictus* embryo by a dominant/negative PDGF receptor. *Development* **124,** 2355–2364.

Rao, K. M., Padmanabhan, J., and Cohen, H. J. (1992). Cytochalasins induce actin polymerization in human leukocytes. *Cell Motil. Cytoskel.* **21,** 58–64.

Sato, M., Schwarz, W. H., and Pollard, T. D. (1987). Dependence of the mechanical properties of actin/α-actinin gels on deformation rate. *Nature* **325,** 828–830.

Sato, M., Theret, D. P., Wheeler, L. T., Ohshima, N., and Nerem, R. M. (1990). Application of the micropipette technique to the measurement of cultured porcine aortic endothelial cell viscoelastic properties. *J. Biomech. Eng.* **112,** 263–268.

Sato, M., Wong, T. Z., Brown, D. T., and Allen, R. D. (1984). Rheological properties of living cytoplasm: A preliminary investigation of squid axoplasm (*Loligo pealei*). *Cell Motil.* **4,** 7–23.

Schliwa, M. (1982). Action of cytochalasin D on cytoskeletal networks. *J. Cell Biol.* **92,** 79–91.

Schmid-Schonbein, G. W., Sung, K. L., Tozeren, H., Skalak, R., and Chien, S. (1981). Passive mechanical properties of human leukocytes. *Biophys. J.* **36,** 243–256.

Schoenwolf, G. C., Folsom, D., and Moe, A. (1988). A reexamination of the role of microfilaments in neurulation in the chick embryo. *Anat. Rec.* **220,** 87–102.

Seybold, Z. V., Mariassy, A. T., Stroh, D., Kim, C. S., Gazeroglu, H., and Wanner, A. (1990). Mucociliary interaction *in vitro:* Effects of physiological and inflammatory stimuli. *J. Appl. Physiol.* **68,** 1421–1426.

Skalak, R., Tozeren, A., Zarda, R. P., and Chien, S. (1973). Strain energy function of red blood cell membranes. *Biophys. J.* **13,** 245–264.

Sokal, R. R., and Rohlf, F. J. (1981). "Biometry." Freeman, New York.

Spiegel, E., Howard, L., and Spiegel, M. (1989). Extracellular matrix of sea urchin and other marine invertebrate embryos. *J. Morphol.* **199,** 71–92.

Sung, K. L., Sung, L. A., Crimmins, M., Burakoff, S. J., and Chien, S. (1988). Dynamic changes in viscoelastic properties in cytotoxic T-lymphocyte-mediated killing. *J. Cell Sci.* **91,** 179–189.

Tanner, C., Frambach, D. A., and Misfeldt, D. S. (1983). Transepithelial transport in cell culture. A theoretical and experimental analysis of the biophysical properties of domes. *Biophys. J.* **43,** 183–190.

Ting-Beall, H. P., Lee, A. S., and Hochmuth, R. M. (1995). Effect of cytochalasin D on the mechanical properties and morphology of passive human neutrophils. *Ann. Biomed. Eng.* **23,** 666–671.

Wainwright, S. A. (1988). "Axis and Circumference: The Cylindrical Shape of Plants and Animals." Harvard Univ. Press, Cambridge, MA.

Wainwright, S. A., Biggs, W. D., Currey, J. D., and Gosline, J. M. (1976). "Mechanical Design in Organisms." Wiley, New York.

Wang, N., Butler, J. P., and Ingber, D. E. (1993). Mechanotransduction across the cell surface and through the cytoskeleton. *Science* **260,** 1124–1127.

Wessel, G. M., Berg, L., Adelson, D. L., Cannon, G., and McClay, D. R. (1998). A molecular analysis of hyalin—A substrate for cell adhesion in the hyaline layer of the sea urchin embryo. *Dev. Biol.* **193,** 115–126.

Wessel, G. M., and McClay, D. R. (1987). Gastrulation in the sea urchin embryo requires the deposition of crosslinked collagen within the extracellular matrix. *Dev. Biol.* **121,** 149–165.

White, F. M. (1991). "Viscous Fluid Flow." McGraw-Hill, New York.

Received for publication July 22, 1998
Revised February 16, 1999
Accepted February 16, 1999